J. Marine Sci. Appl. (2016) 15
DOI: 10.1007/s11804-016-1355-9

Parametric Study on the Effects of Pile Inclination Angle on the Response of Batter Piles in Offshore Jacket Platforms

Ali Aminfar[1], Hamid Ahmadi[2*] and Mohammad Hossein Aminfar[2]

1. Department of Civil Engineering, Tabriz Branch, Islamic Azad University, Pasdaran Highway, Tabriz 5157944533, Iran
2. Faculty of Civil Engineering, University of Tabriz, 29 Bahman Blvd., Tabriz 5166616471, Iran

Abstract: Offshore jacket-type platforms are attached to the seabed by long batter piles. In this paper, results from a finite element analysis, verified against experimental data, are used to study the effect of the pile's inclination angle, and its interaction with the geometrical properties of the pile and the geotechnical characteristics of the surrounding soil on the behavior of the inclined piles supporting the jacket platforms. Results show that the inclination angle is one of the main parameters affecting the behavior of an offshore pile. We investigated the effect of the inclination angle on the maximum von Mises stress, maximum von Mises elastic strain, maximum displacement vector sum, maximum displacement in the horizontal direction, and maximum displacement in the vertical direction. The pile seems to have an operationally optimal degree of inclination of approximately 5°. By exceeding this value, the instability in the surrounding soil under applied loads grows extensively in all the geotechnical properties considered. Cohesive soils tend to display poorer results compared to grained soils.

Keywords: pile, inclination angle, finite element analysis, offshore jacket platform, pile-soil interaction, settlement, offshore piles

Article ID:

1 Introduction

Jacket platforms commonly used for oil and gas extraction are secured to the sea floor with long piles. The offshore structures industry has been flourishing since 1940s (Mao *et al*., 2015). A jack-up platform, with its particular structure, showed obvious dynamic characteristics under complex environmental loads in extreme conditions (Yu e*t al*., 2012). Jackets play a vital role in the offshore industry in field development and operation, with proven flexibility and cost effectiveness (Korzani and Aghakouchak, 2015). Fixed steel offshore platforms are generally composed of a deck with one or more levels, resting on top of a steel jacket (Ferrante *et al.*, 1980). The major structural details incorporated into models of jacket skirt-pile sleeves include the jacket bracing, jacket leg, yoke plate, shear plate, and pile sleeves (Bao and Feng, 2011). In order to define the bearing capacity of the piles, their angles of inclination to the horizon and their diameter and lengths are generally examined. Numerical methods have been widely used in the offshore piling industry for at least the past three decades (Al-Obaid, 1986). Pile founded fixed steel jacket platforms face uncertain modeling variability and sensitivity to seismic response parameters (El-Din and Kim, 2014). Insufficient design of the foundations against such loads can result in disasters (Chen *et al.*, 2015).

In recent years, with the development of the marine petroleum industry, thousands of offshore jacket platforms and other offshore structures have been built (Pan and Zhang, 2009). An inevitable consequence of continued developments in the offshore petroleum industry is the eventual obsolescence of large offshore structures (Pan and Zhang, 2009). Many studies have been conducted to examine the response of these types of piles to various types of loading. In general, nonlinear pile–soil interaction has been identified as the most important source of the nonlinear responses of offshore platforms in designed environmental loads. The interaction between steel and the seafloor involves a number of complexities (Liang, 2009). Researchers have concluded that the lateral cyclic deflection of the platform using cyclic backbone curves is considerably higher than the corresponding results under monotonic loads. Furthermore, pile responses (deflections, shear forces, and bending moments) for cyclic curves are more sensitive to cyclic loads than pile results using static backbone curves (Memarpour *et al.*, 2012). The most favorable capacity is achieved when pile–soil interaction is considered in the analysis. This means that the use of linear pile stubs is recommended for the initial stiffness assessment but it is not recommended for the ultimate strength assessment (Asgarian and Lesani, 2009).

The necessity of evaluating the pull-out capacity of batter piles in coastal environments is basically due to the overturning moments from wind load, wave pressure, and ship impacts on the offshore structures and to the retaining walls that are subjected to horizontal forces and bending moments from earth pressures. Furthermore, a pile's embedment ratio has a significant effect on the pullout capacity of the batter pile, and the resistances offered by a pile at any axial displacement increases significantly with an increase in this ratio. However, rough-model piles experience 18%–75% increases in capacity compared with smooth-model piles. The ultimate pullout capacity of a batter pile constructed in loose sand decreases with an

Received date: 2015-09-20
Accepted date: 2015-12-23
***Corresponding author Email:** h-ahmadi@tabrizu.ac.ir

increasing pile batter angle (Nazir and Nasr, 2012). Traditional models use well-known semi-empirical approaches in which the soil response is characterized as an independent nonlinear spring at discrete locations. As such, these models do not account for pile bending stiffness or the interaction of the pile–soil system (Sangseom *et al.*, 2009; 2011).

The stress distribution within a large structure such as a Tension Leg Platform (TLP) is a dominant factor in the design procedure of an offshore pile. The loading of an offshore structure consists of two vertical structural loads and lateral wave loads. As the wave period increases the peak displacement of the pile significantly decreases, so shorter wave periods have a more critical effect on pile displacement. Furthermore, increasing wave heights create a dramatic increase on the peak displacement, while minimum stresses actually decrease significantly (Eicher *et al*., 2003). A pile fails when the maximum bending moment acting on a critical section is greater than the ultimate bending capacity of that section (Ruiz, 1984).

In this paper, we consider the results of Finite Element (FE) analysis using ANSYS, verified against experimental data, to study the effects of the pile's inclination angle, and its interaction with the geometrical properties of the pile and geotechnical characteristics of the surrounding soil, on the behavior of the inclined piles supporting the jacket platforms. Results show that the inclination angle is one of the main parameters affecting the behavior of an offshore pile. Here we study the effect of inclination angle on the maximum von Mises stress, maximum von Mises elastic strain, maximum displacement vector sum, maximum displacement in the horizontal direction, and maximum displacement in the vertical direction.

2 Finite element modeling

2.1 Geometrical modeling

In order to develop an FE model with ANSYS software, we first need to generate a medium for the geometry of the model and identify and define the required model elements (as shown in Fig. 1).

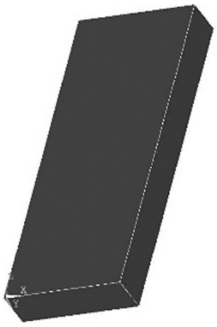

Fig. 1 Generated medium (pile diameter: 0.5 m, pile inclination: 18°)

We defined the parameter θ (in degrees) as the inclination angle of the pile with respect to the *XY* plane. Next, we introduced the length of the pile to the software (in this study, 30 m). The length of the soil medium is in the *Y* direction.

In order to define the width of the soil medium, the inclination of the pile must be taken into consideration. As the pile is oriented in the *X* direction, the volume of medium needed to contain the pile will expand. The elevation in the *Z* direction has been set as maximum in all the situations by taking the length of the pile and adding an extra 4 meters to assure that the model behavior will not be altered by any increase in elevation. Now, we can cube the given dimensions in the software.

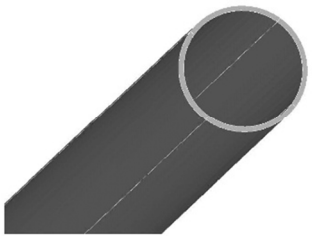

Fig. 2 Modeled pile (diameter: 0.5 m)

Next, we used the software to generate a cylindrical coordinate system with its origin in the pile's end with coordinates of (4, 2, 2) (the bottom of the pile located in the soil) and its axes having θ degrees of inclination with the *Z* axis of the original coordinate system. The outer diameters considered for the piles were 50, 60, and 70 cm (Fig. 2).

2.2 Meshing

After defining the volumes, we could then apply the meshing. We chose tetrahedral meshes for this study mainly because of the model's non-uniform shape. Introducing this type of mesh would not be possible without considering the assumptions of the solid 186 environment. The pile and the soil media were meshed individually and then merged. The solid 186 element had 20 nodes in all three dimensions, allowing for easy study of the element behavior with multiple degrees of freedom and three degrees of freedom per node (its movement in the *X*, *Y* and *Z* directions) (Fig. 3).

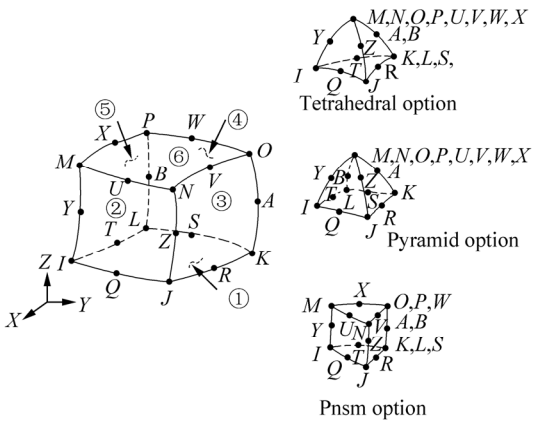

Fig. 3 ANSYS element type Solid 186

2.3 Material properties

The steel used to define the pile has properties consistent with the ASTM A36 (2004) standard, with a specific weight of 7 700 kg/m^3. The other ASTM-A36 steel parameters are listed in Table 1.

Table 1 Steel material designation according to ASTM A36 (2004)

Property	Variable	Value
Young's modulus	EX/(N·m^{-2})	2E+11
	EY/(N·m^{-2})	2E+11
	EZ/(N·m^{-2})	2E+11
Poisson's ratio	NUXY	0.3
	NUYZ	0.3
	NUXZ	0.3
Shear modulus	GXY/(N·m^{-1})	7.7E+10
	GYZ/(N·m^{-1})	7.7E+10
	GXZ/(N·m^{-1})	7.7E+10

To define the soil materials, the non-linear behavior of the soil must be introduced to the software, and we chose the Drucker–Prager model to do so. Here, we briefly introduce this model (Helwany, 2007).

The Drucker–Prager/cap plasticity model has been widely used in finite element analysis programs for a variety of geotechnical engineering applications. The cap model is appropriate for soil behavior because it can consider the effects of stress history, stress path, dilatancy, and the intermediate principal stress. The yield surface of the modified Drucker–Prager/cap plasticity model consists of three parts: a Drucker–Prager shear failure surface, an elliptical cap, which intersects the mean effective stress axis at a right angle, and a smooth transition region between the shear failure surface and the cap, as shown in Fig. 4.

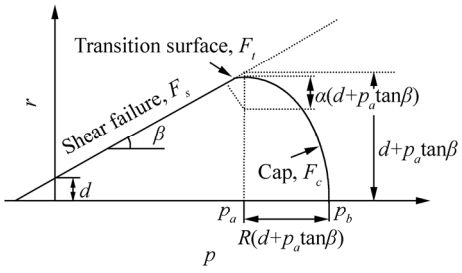

Fig. 4 Yield surfaces of the modified cap model in the *p–t* plane (Helwany, 2007)

Elastic behavior is modeled as linear elasticity using the generalized Hooke's law. Alternatively, an elasticity model in which the bulk elastic stiffness increases as the material undergoes compression can be used to calculate the elastic strains (Eq. (1)). The onset of plastic behavior is determined by the Drucker–Prager failure surface and the cap yield surface. The Drucker–Prager failure surface is given by:

$$Fs = t - p\tan\beta - d = 0 \tag{1}$$

where β is the soil's angle of friction and d is its cohesion in the *p–t* plane (*p* is the stress and t is the strain), as indicated in Fig. 4. As shown in the figure. , the cap yield surface is an ellipse with eccentricity =*R* in the *p–t* plane. The cap yield surface is dependent on the third stress invariant, *r*, in the deviatoric plane, as shown in Fig. 4 (Eqs. (2) and (3)). J_1, J_2 and J_3 are the invariants of the stress tensor and J_{1D}, J_{2D} and J_{3D} are the invariants of the deviatoric stress tensor.

$$q = \sqrt{3J_{2D}} = \sqrt{3(J_2 - \frac{J_1^2}{6})} = \sqrt{\frac{1}{2}[(\sigma_1-\sigma_2)^2 + (\sigma_2-\sigma_3)^2 + (\sigma_1-\sigma_3)^2]} \tag{2}$$

$$r = (\frac{27}{2}J_{3D})^{1/3} = (\frac{27}{2}J_3 - 9J_1J_2 + J_1^3)^{1/3} \tag{3}$$

The cap surface hardens (expands) or softens (shrinks) as a function of the volumetric plastic strain. When the stress state causes yielding on the cap, volumetric plastic strain (compaction) causes the cap to expand (hardening). However, when the stress state causes yielding on the Drucker–Prager shear failure surface, volumetric plastic dilation occurs, causing the cap to shrink (softening). The cap yield surface is given as

$$F_c = \sqrt{(p-p_a)^2 + (\frac{Rt}{1+\alpha-\alpha/\cos\beta})^2} - R(d+P_a\tan\beta) = 0 \tag{4}$$

where *R* is a material parameter that controls the shape of the cap and α is a small number (typically 0.01 to 0.05) used to define the smooth transition surface between the Drucker–Prager shear failure surface and the cap:

$$F_t = \sqrt{(p-P_a)^2 + [t-(1-\frac{\alpha}{\cos\beta})(d+P_a\tan\beta)]^2} - \alpha(d+P_a\tan\beta) = 0 \tag{5}$$

P_a is an evolution parameter that controls the hardening–softening behavior as a function of the volumetric plastic strain. The hardening–softening behavior is simply described by a piecewise linear function relating the mean effective (yield) stress P_b and the volumetric plastic strain P_b=(ε^{pl}_{vol}), as shown in Fig. 5. This function can easily be obtained from the results of one isotropic consolidation test with several unloading–reloading cycles. Consequently, the evolution parameter, P_a, can be calculated as

$$P_a = \frac{P_b - Rd}{1 + R\tan\beta} \tag{6}$$

The flow potential is identical to the yield surface (i.e., associated flow). For the Drucker–Prager failure surface and the transition yield surface, a nonassociated flow is assumed: The shape of the flow potential in the *p–t* plane is different

from that of the yield surface, as shown in Fig. 6. In the cap region, the elliptical flow potential surface is given as

$$G_c = \sqrt{(p - p_a)^2 + \left(\frac{Rt}{1 + \alpha - \alpha/\cos\beta}\right)^2} \quad (7)$$

The elliptical flow potential surface portion in the Drucker–Prager failure and transition regions is given as

$$G_S = \sqrt{[(p_a - p)\tan\beta]^2 + \left(\frac{t}{1 + \alpha - \alpha/\cos\beta}\right)^2} \quad (8)$$

As shown in Fig. 7, the two elliptical portions, G_c and G_s, provide a continuous potential surface. Because of the nonassociated flow used in this model, the material stiffness matrix is not symmetric. Thus, an unsymmetrical solver should be used in association with the cap model.

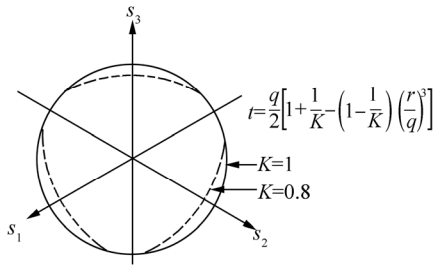

Fig. 5 Projection of the modified cap yield/flow surfaces on the Π-plane (Helwany, 2007)

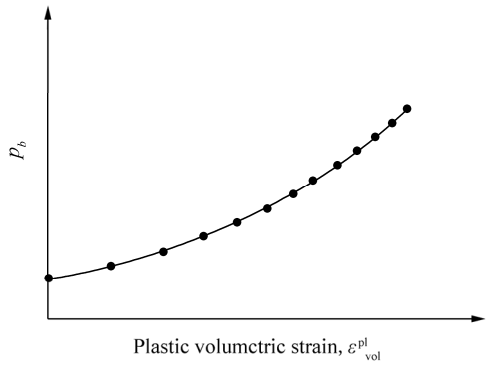

Fig. 6 Typical cap hardening behavior (Helwany, 2007)

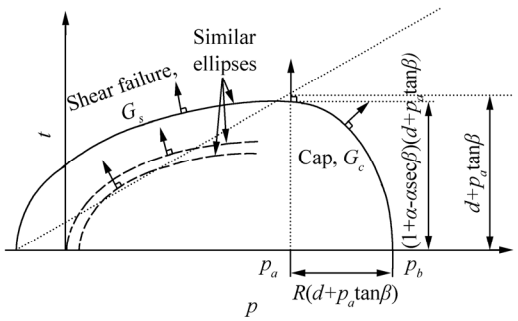

Fig. 7 Flow potential of the modified cap model in the *p–t* plane (Helwany, 2007)

The results of at least three triaxial compression tests are required to determine the parameters d and β. The at-failure conditions taken from the tests results can be plotted in the *p–t* plane. A straight line is then best fitted to the three (or more) data points. The intersection of the line with the *t*-axis is d and the slope of the line is β. We also need the results of one isotropic consolidation test with several unloading–reloading cycles, which can be used to evaluate the hardening–softening law as a piecewise linear function relating the hydrostatic compression yield stress P_b and the corresponding volumetric plastic strain $P_b=(\varepsilon^{pl}_{vol})$ (Fig. 5). The unloading–reloading slope can be used to calculate the volumetric elastic strain that should be subtracted from the volumetric total strain when calculating the volumetric plastic.

Table 2 lists the parameters needed to define the nonlinear soil characteristics, in accordance with the Drucker-Prager/cap model. We analyzed three types of soil, a totally cohesive soil (φ=0 and ψ=0, type A), a totally non-cohesive soil (C=0, type C), and an even mixture of both (type B).

Table 2 Soil characteristics

Variable	Value
Cohesion (C and d)/(N·m^{-2})	3 400
Angle of friction (φ and β)/(°)	38
Angle of dilation (ψ)/(°)	38
EXY/(N·m^{-2})	2E+11
EYZ/(N·m^{-2})	2E+11
EXZ/(N·m^{-2})	2E+11
NUXY	0.3
NUYZ	0.3
NUXZ	0.3
GXY/(N·m^{-1})	7.7E+010
GYZ/(N·m^{-1})	7.7E+010
GXZ/(N·m^{-1})	7.7E+010
γ_{sat}/(N·m^{-3})	11 800

2.4 Loading and analysis

After applying the mesh, we then applied a surface load of 2E+08 (N/m^2) to the upper ring of the pile, and executed the solver.

2.5 Verification

Zou *et al.* (2007), Zou and Zhao (2013) have studied long pipe piles in different multilayered soil environments and have conducted actual tests on these pile systems. More recently, the authors have mathematically modeled their system using the Element-Free Galerkin Method (EFGM). In their study, the pipe pile had a diameter of 1m and a length of 60 m. Despite the fact that their pipe was made of reinforced concrete, they used weight average values to determine the piles' elastic modules and tensile strengths.

To verify the FE models, we used the results of Zou *et al.* (2007), and extracted the soil layers and geotechnical parameters from their paper mentioned above. The FE analysis results from the present study and those from the study by Zou *et al.* (2007) are shown in Fig. 8.

As indicated in the figure, the maximum difference between the FE results of the present study and the measured values from the actual model is less than 8%. The FE model performs even better when compared with the element-free Galerkin model. Hence, we can conclude that the FE models developed here are sufficiently accurate to produce valid results.

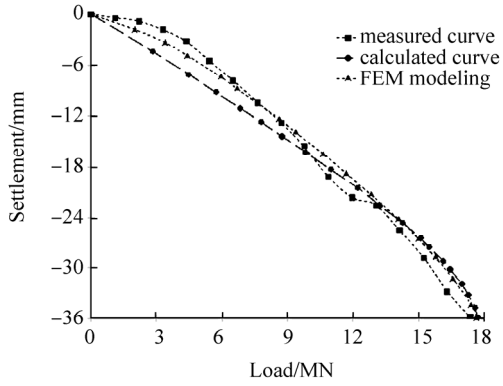

Fig. 8 Verification of FE results using the experimental data (measured curve) and results of element free Galerkin method (calculated curve) provided by Zou *et al*. (2007)

3 Results and discussion

Fig. 9 shows the change in the maximum von Mises stress owing to the increased pile inclination angle. This figure includes results from the three considered soil types (A, B, and C) and three considered pile diameter values (0.5, 0.6, and 0.7 m). We can see that the maximum von Mises stress increases by increasing the pile diameter. While the amount of this increase is considerable for piles facing inclinations of more than 9°, the stress margin in piles with inclination degrees less than 8° is not significant. By increasing the inclination of the pile, the maximum von Mises stress grows rapidly to 6 times its initial value, mainly owing to the deformation of the pile in certain areas.

The growth is steady at first, climbing gently until 7°. After that, the growth distribution is more rapid and exhibits a parabolic behavior, in contrast to the more linear trend of the increase for smaller degrees of inclination. For inclinations more than 18°, a change in pile diameter seems to have a more tangible effect on the von Mises stress. Furthermore, the trend of increase in the stress values for cohesive soils is slightly lower than for soils having grained particulates.

Fig. 10 depicts the change of the maximum von Mises elastic strain owing to the increase of the inclination angle of the pile. We can see that the maximum von Mises elastic strain is increased in piles having bigger diameters. As seen in the maximum von Mises stress, piles with inclinations of less than 5° exhibit only a small difference when the pile diameter changes. This increase is more dramatic for inclinations more than 7°. However, the trend of this increase seems to be the same for all pile diameters. The maximum elastic von Mises strain gradually increases to double its original value at an inclination of about 7°. Furthermore, the increase rate for piles with more than 7° of inclination is extremely rapid in comparison to the initial increase rate. The increase in the pile's maximum strain reaches its peak at eight times its initial value. The surfaces indicate a semilinear increase trend for all soil types with inclinations less than 7°. However, soils with more cohesive characteristics show lower strain dilations. The steady increase in the elastic strain surfaces are followed by sharp increases at inclinations of more than 9° that are showing little sensitivity to soil-type fluctuations.

Fig. 11 illustrates the change in the vector sum of the maximum displacement owing to the increase of the pile inclination angle. We can observe that the vector sum of the maximum displacement has a parabolic shape for all pile diameters, with its minimum at 4°. The increase rate of maximum displacement is less sensitive to inclinations lower than 6°, and exhibits less fluctuation. By contrast, for inclinations of more than 7°, the rate increases in piles with greater diameters. The shape of the parabolic surface with respect to the vector sum of the maximum displacement of the pile indicates a slight increase in the overall displacement of the pile at inclinations of less than 4 degrees. The rate of increase of the overall displacement starts from a minimum at 4°, and remains gentle until 7°. At inclinations of more than 7°, the increase in the vector sum of the maximum displacement is stronger, growing to three times the minimum displacement.

The vector sum of the maximum displacement, or in other words, the total displacement, surfaces suggest slightly greater displacements for cohesive soils. However, with the increase of inclination from 9°, the displacement margin shows rapid growth, as compared to inclinations of less than 7° for all soil types.

Fig. 12 indicates the change in maximum displacement in the horizontal direction owing to the increase of the pile inclination angle. We consider the maximum displacement in the horizontal direction here in order to examine the pile's lateral response. First, the curves suggest a parabolic shape with a minimum at 4° of inclination.

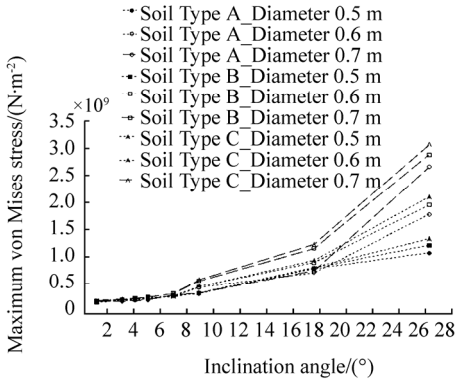

Fig. 9 The effect of pile inclination angle on the maximum von Mises stress

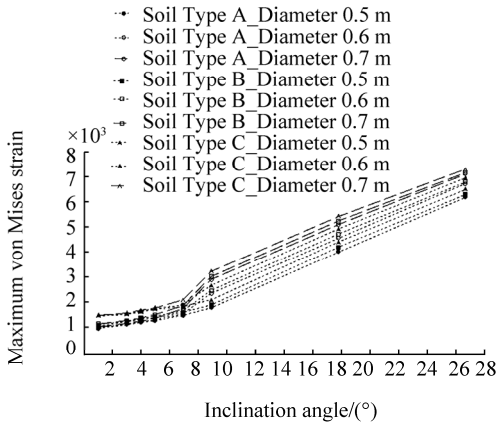

Fig. 10 The effect of pile inclination angle on the maximum von Mises elastic strain

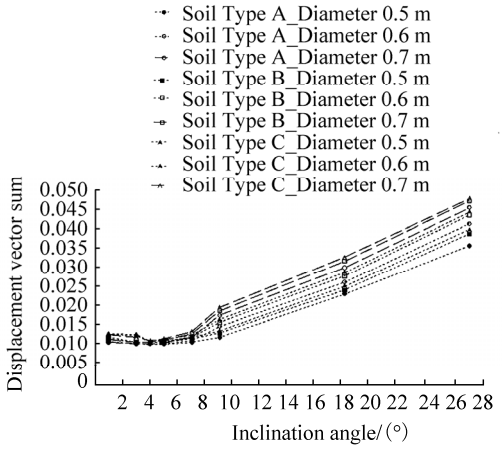

Fig. 11 The effect of pile inclination angle on the displacement vector sum

The most considerable difference between the lateral response of the pile to its total and settlement responses is that the pile is not sensitive to diameter change. This means that by increasing the diameter, the pile undergoes only slight fluctuations. This pattern of constancy is important for inclinations of more than 7°, because in such scenarios the difference between the responses of the pile to loading is considerable with respect to diameter changes. Second, the parabolic shape of the curves indicate a slight decrease in the lateral displacement of the pile when its inclination increases from 1° to 5°. This means that the least and most acceptable lateral response of the pile occurs at 4° to 5°. By increasing the inclination of the pile, the increase rate in the pile's lateral response for inclination increases from 5° to 9° is considered to be slight compared to its response to higher inclinations. Higher inclination angles result in further lateral displacement. The least lateral response for all soil types occurs at 5° of inclination. Furthermore, all soil types behave similarly at low inclinations. However, after the 9° of inclination, cohesive soils exhibit lower lateral dilations.

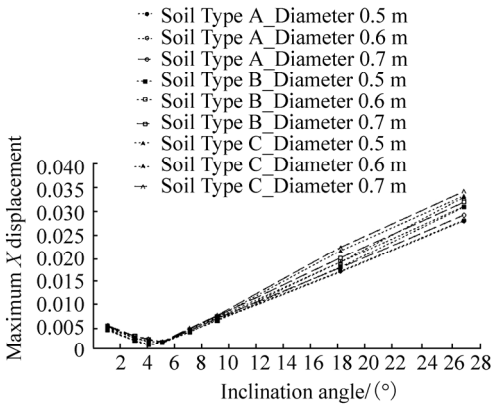

Fig. 12 The effect of pile inclination angle on the maximum horizontal displacement

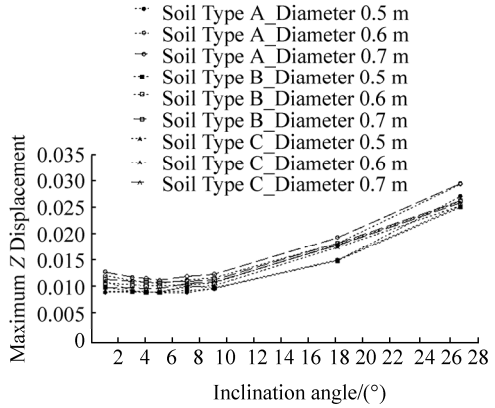

Fig. 13 The effect of pile inclination angle on the maximum vertical displacement

Fig. 13 shows the change in the maximum displacement in the vertical direction owing to the increase of the pile inclination angle. The maximum displacement in the vertical direction, or in other words the settlement, decreases as the weight of the pile itself decreases. In other words, piles with a lower diameter exhibit slightly better behavior when it comes to their maximum displacements in the vertical direction. The settlement surface consists of two phases, the first for inclinations from 1° to 9° and the next for angles of more than 9°. The first phase has a constant trend, which means that settlements in this phase do not fluctuate strongly. However, piles with inclination angles between 4° and 5° exhibit even lower settlements than those with other degrees of inclination during the same phase. In the second phase, a sharp increase occurs in the settlement pattern. The increase pattern itself has a linear trend. Changes in the soil types result in very visible differences at slight degrees of inclination, showing greater settlement in cohesive soils. However, changes in the soil's geotechnical characteristics result in decreased settlements as the degree of inclination of the pile increases. For extreme inclinations, the settlement of the pile shows similar behavior to piles with very slight inclinations, with more settlement in cohesive soils.

4 Conclusions

In this paper, we used FE analysis results, verified against experimental data, to study the effects of pile inclination angle, and its interaction with the geometrical properties of the pile and the geotechnical characteristics of the surrounding soil, on the behavior of inclined piles that support jacket platforms. The main conclusions can be summarized as follows:

The inclination angle is one of the main parameters affecting the behavior of an offshore pile. The effect of the inclination angle on the maximum von Mises stress, maximum von Mises elastic strain, maximum displacement vector sum, maximum displacement in the horizontal direction, and maximum displacement in the vertical direction were extensively discussed. The pile exhibits what seems to be an optimal operational inclination of about 5°. By exceeding this optimum degree of inclination, instability of the geotechnical properties of the surrounding soil under applied loads grew extensively in all considered cases. Soils having cohesive characteristics displayed poorer results compared to grained soils. The use of piles with inclination angles of more than 10° must be restricted in structures like dolphins and at waterfronts; and where used in such structures, caution is advised.

Nomenclature

θ/(°)	Inclination angle of the pile
X, Y, Z	Three axes of the coordinate system
EX/(N·m^{-2})	Elastic modulus, element X direction
EY/(N·m^{-2})	Elastic modulus, element Y direction
EZ/(N·m^{-2})	Elastic modulus, element Z direction
NUXY	Poisson's ratio, X-Y plane
NUYZ	Poisson's ratio, Y-Z plane
NUXZ	Poisson's ratio, X-Z plane
GXY/(N·m^{-1})	Shear modulus, X-Y plane
GYZ/(N·m^{-1})	Shear modulus, Y-Z plane
GXZ/(N·m^{-1})	Shear modulus, X-Z plane
C , d/(N·m^{-2})	Cohesion
φ, β/(°)	Angle of friction
ψ/(°)	Angle of dilation
γ_{sat}	Special weight (saturated)
p and σ	Stress
t	Strain
r	Third stress invariant
j_x	x invariant of the stress tensor
J_{xD}	x invariant of the deviatoric stress tensor
F_c	Cap failure surface
F_t	Transition surface
F_s	Shear failure surface
R	Material parameter controlling the shape of the cap
α	Smooth transition parameter
P_a	Evolution parameter
P_b	Mean effective (yield) stress
ε^{pl}_{vol}	Volumetric plastic strain
G_c	Elliptical flow potential surface in the cap region
G_s	Elliptical flow potential surface in the Drucker–Prager failure and transition regions

References

Al-Obaid YF, 1986. Numerical analysis of the laterally loaded piles in the Kuwait offshore environment. *Ocean Engineering*, **13**(1), 85-92.
DOI: 10.1016/0029-8018(86)90005-3

Asgarian B, Lesani M, 2009. Pile-soil-structure in pushover analysis of jacket offshore platforms using fiber elements. *Journal of Construction Steel Research*, **65**(1), 209-218.
DOI: 10.1016/j.jcsr.2008.03.013

ASTM A36, 2014. *Standard specification for carbon structural steel*. ASTM International, Conshohocken, USA, Designation A 36/A 36M-97a, 46 CFR 160.035-3(b) (2).
DOI: 10.1520/A0036_A0036M-14

Bao Q, Feng H, 2011. Finite element simplified fatigue analysis method for a non-tubular joint of an offshore jacket platform. *Journal of Marine Science and Application*, **10**(3), 321-324.
DOI: 10.1007/s11804-011-1075-0

Chen Y, Gu M, Chen R, Kong L, Zhang Z, Bian X, 2015. Behavior of pile group with elevated cap subjected to cyclic lateral loads. *China Ocean Engineering*, **29**(4), 565-578.
DOI: 10.1007/s13344-015-0039-6

Eicher JA, Guan H, Jeng DS, 2003. Stress and deformation of offshore piles under structural and wave loading. *Ocean Engineering*, **30**(3), 369-385.
DOI: 10.1016/S0029-8018(02)00031-8

El-Din MN, Kim J, 2014. Sensitivity analysis of pile-founded fixed steel jacket platforms subjected to seismic loads. *Ocean Engineering*, **85**(1), 1-11.
DOI: 10.1016/j.oceaneng.2014.04.008

Ferrante AJ, Valenzula EC, Ellwanger GB, 1980. An integrated computational procedure for the analysis of offshore structures supported by piles. *Advanced Engineering Software*, **2**(4), 169-172.
DOI: 10.1016/0141-1195(80)90050-9

Helwany S, 2007. *Applied soil mechanics with Abaqus applications*. John Wiley & Sons, Hoboken Incorporation, Hoboken, USA, 60-64.

Korzani MG, Aghakouchak AA, 2015. Soil-structure interaction analysis of jack-up platforms subjected to monochrome and irregular waves. *China Ocean Engineering*, **29**(1), 65-80.
DOI: 10.1007/s13344-015-0005-3

Liang H, 2009. Review of research on interactions between deepwater steel catenary risers and soft clay seabeds. *Journal of Marine Science and Application*, **8**(1), 163-167.
DOI: 10.1007/s11804-009-8115-z

Mao D, Zhong C, Zhang L, Chu G, 2015. Dynamic response of offshore jacket platform including foundation degradation under cyclic loadings. *Ocean Engineering*, **100**(1), 35-45.
DOI: 10.1016/j.oceaneng.2015.03.012

Memarpour MM, Kimiaei M, Shayanfar M, Khanzadi M, 2012. Cyclic lateral response of pile foundations in offshore platforms. *Computers and Geotechnics*, **42**(1), 180-192.
DOI: 10.1016/j.compgeo.2011.12.007

Nazir A, Nasr A, 2014. Pullout capacity of batter pile in sand. *Journal of Advanced Research*, **4**(2), 147-154.

DOI: 10.1016/j.jare.2012.04.001

Pan X, Zhang Z, 2009. Analyzing the safety of removal sequences for piles of an offshore jacket platform. *Journal of Marine Science and Application*, **8**(4), 311-315.
DOI: 10.1007/s11804-009-8050-z

Sangseom J, Donghee S, Youngho K, 2009. Numerical analysis of passive pile groups in offshore deposits. *Computers and Geotechnics*, **36**(7), 1164-1175.
DOI: 10.1016/j.compgeo.2009.05.003

Sangseom J, Youngho K, Jaeyoung K, 2011. Influence on lateral rigidity of offshore piles using proposed p-y curves. *Ocean Engineering*, **38**(2-3), 397-408.
DOI: 10.1016/j.oceaneng.2010.11.007

Ruiz SE, 1984. Reliability index for offshore piles subjected to bending. *Structural Safety*, **2**(2), 83-90.
DOI: 10.1016/0167-4730(84)90012-2

Yu Hao, Li Xiaoyu, Yang Shuguang, 2012. Dynamic analysis method of offshore jack-up platforms in regular and random waves. *Journal of Marine Science and Application*, **11**(1), 111-118.
DOI: 10.1007/s11804-012-1112-7

Zou X, Zhao M, 2013. Axial bearing behavior of super-long piles in deep soft clay over stiff layers. *Journal of Central South University of Technology*, **20**(7), 2008-2016.
DOI: 10.1007/s11771-013-1702-9

Zou X, Zhao M, Liu G, 2007. Buckling analysis of super-long rock-socketed filling piles in soft soil area by element free Galerkin method. *Journal of Central South University of Technology*, **14**(6), 858-863.
DOI: 10.1007/s11771-007-0163-4